Applications of Mathematics

Mária Lukáčová-Medviďová; Jitka Saibertová

Finite volume schemes for multi-dimensional hyperbolic systems based on the use of bicharacteristics

Applications of Mathematics, Vol. 51 (2006), No. 3, 205–228

Persistent URL: http://dml.cz/dmlcz/134637

51 (2006) APPLICATIONS OF MATHEMATICS No. 3, 205–228

FINITE VOLUME SCHEMES FOR MULTI-DIMENSIONAL HYPERBOLIC SYSTEMS BASED ON THE USE OF BICHARACTERISTICS*

Mária Lukáčová-Medviďová, Hamburg,
Jitka Saibertová-Zatočilová, Brno

(Received March 28, 2004, in revised version August 24, 2004)

Abstract. In this paper we present recent results for the bicharacteristic based finite volume schemes, the so-called finite volume evolution Galerkin (FVEG) schemes. These methods were proposed to solve multi-dimensional hyperbolic conservation laws. They combine the usually conflicting design objectives of using the conservation form and following the characteristics, or bicharacteristics. This is realized by combining the finite volume formulation with approximate evolution operators, which use bicharacteristics of the multi-dimensional hyperbolic system. In this way all of the infinitely many directions of wave propagation are taken into account. The main goal of this paper is to present a self-contained overview on the recent results. We study the L^1-stability of the finite volume schemes obtained by various approximations of the flux integrals. Several numerical experiments presented in the last section confirm robustness and correct multi-dimensional behaviour of the FVEG methods.

Keywords: multidimensional finite volume methods, bicharacteristics, hyperbolic systems, wave equation, Euler equations

MSC 2000: 76M12, 35L65, 35L45, 65M12, 65M25, 65M60

1. Introduction

In general, numerical solution of truly multi-dimensional systems of conservation laws is a challenging task. The main reason is that even for small initial data we do not have existence and qualitative results for the solution of multi-dimensional

* This research has been supported under the VW-Stiftung grant I 76 859, by the grant No 201/03 0570 of the Grant Agency of the Czech Republic, by the Deutsche Forschungsgemeinschaft grant GK 431 and partially by the European network HYKE, funded by the EC as contract HPRN-CT-2002-00282.

Riemann problems. In principle, we have two finite volume approaches to overcome this fact. First, there are the so-called central finite volume methods (FVM), which do not use the Riemann problem, see e.g. [4] and the references therein. However, if no characteristic information is taken into account they may not provide a satisfactory resolution when small time steps are enforced by the stability condition. Note that for multi-dimensional problems the central schemes have the CFL stability restrictions strongly less than 1.

The second approach is based on a quasi-dimensional splitting and on the use of an approximate solution to the one-dimensional Riemann problem, with well understood structure. If the main features we want to approximate are just one-dimensional, this approach can produce good qualitative results. But for complex genuinely multi-dimensional structures, such as oblique shocks or circular expansions, dimensional splitting approach can yield spurious local wave structure resolutions.

Looking back to the literature of the last decade we find several new genuinely multi-dimensional methods. For example, the wave propagation algorithm of LeVeque [5], the method of transport (MoT) of Fey [2] and its simplified version of Noelle [14], or the multistate FVM of Brio et al. [1]. The last approach is based on the use of the Kirchhoff formulae for the wave equation or the linearized Euler equations in order to correct multi-dimensional contributions in corners of the computational cells. In fact, our approach is similar to that of Brio. However, instead of the Kirchhoff formulae which are explicit in time but singular over the sonic circle, we use a different method. We work with a general theory of bicharacteristics for linear hyperbolic systems of first order and derive the so-called approximate evolution operators. This is the most involved part of the derivation of our schemes.

The basic idea of the *evolution Galerkin schemes* (EG), introduced by Morton, see e.g. [13], is the following. Transport quantities are shifted along characteristics and then projected onto a finite element space. Using the results of Ostkamp [15] we have derived in [7] several new evolution Galerkin methods for the linear system of the wave equations, which have better stability properties as well as global accuracy. Their generalization to the second order EG method was done in [11] for linear two-dimensional systems. In [6] we have studied the two-dimensional Riemann problem for the wave equation system and demonstrated good accuracy of the EG schemes as well as correct multi-dimensional resolution of oblique shocks.

In her dissertation [16] Ostkamp proposed a generalization of the EG method to nonlinear Euler equations. However, in order to implement her scheme quite tedious calculations of three-dimensional integrals had to be done. It was barely feasible for practical applications, such as the shallow water equations and the Euler equations, especially for higher order methods. The decisive step was to take a different approach, which led us to the finite volume framework. In the so-called

finite volume evolution Galerkin (FVEG) methods the approximate evolutions are used only on cell interfaces to evaluate the numerical fluxes.

Note that there is a connection between the FVEG method and the interface centered MoT of Noelle. Both methods use multi-dimensional evolution only on cell interfaces instead of on whole computational cells. This leads to the crucial simplification of the original methods within the FV framework.

The aim of this paper is to give a self-contained overview on the recent results of the evolution Galerkin schemes. We want to present the basic ideas of the theory of bicharacteristics, which are used for the derivation of exact and approximate evolution operators for general multi-dimensional hyperbolic systems. We illustrate the application of these techniques on the Euler equations system. Further interesting applications are, for example, the wave equation system, the shallow water equations, the magneto-hydrodynamic equations or the equations of nonlinear elasticity.

The paper is organized as follows. In Section 2 the formulation of the finite volume evolution Galerkin scheme is presented. The exact integral representations for the linearized Euler equations are given in Section 3. In order to apply the approximate evolution operator to fully nonlinear systems, such as the Euler equations of gas dynamics or the shallow water equations, first a suitable linearization is needed. It is done by freezing the Jacobian matrices locally around suitable constant states. Despite the linearization procedure the FVEG methods satisfy the entropy condition on sonic rarefaction waves and no entropy fix is needed, see [8], [9] for numerical experiments. Approximation of the so-called mantle integrals is discussed in Section 4. We describe the EG3 approximate evolution operator [7] and following the lines of our recent paper [9] we present new EG5 approximate evolution operators, which yield numerical schemes stable almost up to the CFL number 1. In Section 5 the second order scheme obtained by means of a bilinear recovery in space is introduced. We present here an L^1-stability analysis of the FVM obtained by different cell interface flux integration.

The error analysis of the FVEG methods was presented in [9] and [17]. For linear or linearized systems it was proved that if a bilinear recovery is used the method is of the second order in space and time. In Section 6 we illustrate through numerical experiments the behaviour of the scheme on various test examples.

2. Finite volume evolution Galerkin method

Let Ω be our two-dimensional computational domain covered by regular square mesh cells

$$\begin{aligned}\Omega_{ij} &\equiv \left[\Big(i-\frac{1}{2}\Big)h, \Big(i+\frac{1}{2}\Big)h\right] \times \left[\Big(j-\frac{1}{2}\Big)h, \Big(j+\frac{1}{2}\Big)h\right] \\ &= \big[x_{i-\frac{1}{2}}, x_{i+\frac{1}{2}}\big] \times \big[y_{j-\frac{1}{2}}, y_{j+\frac{1}{2}}\big],\end{aligned}$$

where $i, j \in \mathbb{Z}$, and $h > 0$ is the mesh size parameter.

In finite volume schemes typically the one-dimensional Riemann problems in normal direction to the cell interfaces are used to approximate fluxes on cell interfaces. Instead of this dimensional-splitting technique we use in our scheme a genuinely multi-dimensional approach. In order to compute fluxes on cell interfaces the value of the approximate solution will be determined by means of a suitable approximate evolution operator. In this way all directions of wave propagation are taken into account explicitly.

As an example of general hyperbolic conservation laws let us consider the Euler equations written in the conservative variables

$$\boldsymbol{u}_t + \boldsymbol{f}_1(\boldsymbol{u})_x + \boldsymbol{f}_2(\boldsymbol{u})_y = 0. \tag{2.1}$$

Here the vector of conservative variables is $\boldsymbol{u} := (\varrho, \varrho u, \varrho v, e)^T$ and the fluxes are

$$\boldsymbol{f}_1(\boldsymbol{u}) := \begin{pmatrix} \varrho u \\ \varrho u^2 + p \\ \varrho uv \\ (e+p)u \end{pmatrix}, \quad \boldsymbol{f}_2(\boldsymbol{u}) := \begin{pmatrix} \varrho v \\ \varrho uv \\ \varrho v^2 + p \\ (e+p)v \end{pmatrix},$$

where ϱ is the density, ϱu, ϱv is the momentum in x-, y-direction, respectively, p is the pressure and e stands for the total energy, i.e. $e = p/(\gamma - 1) + \varrho(u^2 + v^2)/2$.

Let us integrate (2.1) over a mesh cell Ω_{ij} and time interval $[t_n, t_{n+1}]$. Applying the Gauss theorem for the flux integrals yields the equality

$$\int_{\Omega_{ij}} \boldsymbol{u}(x,y,t)\,\mathrm{d}x\,\mathrm{d}y\Big|_{t_n}^{t_{n+1}} + \int_{t_n}^{t_{n+1}} \int_{\partial\Omega_{ij}} (\boldsymbol{f}_1(\boldsymbol{u})n_x + \boldsymbol{f}_2(\boldsymbol{u})n_y)\,\mathrm{d}S\,\mathrm{d}t = 0, \tag{2.2}$$

where (n_x, n_y) is the unit outer normal to the face of the control volume $\partial\Omega_{ij}$. Let $\boldsymbol{U}^{n+1}, \boldsymbol{U}^n$ denote the piecewise constant functions obtained by the integral averages evaluated at time t_{n+1} or t_n, respectively. More precisely,

$$\boldsymbol{U}^n\Big|_{\Omega_{ij}} = \frac{1}{h^2} \int_{\Omega_{ij}} \boldsymbol{u}(x,y,t_n)\,\mathrm{d}x\,\mathrm{d}y.$$

The crucial point of the FVEG schemes is the use of the approximate evolution operators for the evaluation of fluxes at cell interfaces.

Starting from some initial data $\boldsymbol{U}^0$ at time $t = 0$ and taking into account the fact that the regular rectangular mesh is used, the finite volume evolution Galerkin method (FVEG) is recursively defined by means of

$$\boldsymbol{U}^{n+1} = \boldsymbol{U}^n - \frac{1}{h}\int_{t_n}^{t_{n+1}} \boldsymbol{F}_1(\boldsymbol{U}(t))\,\mathrm{d}t - \frac{1}{h}\int_{t_n}^{t_{n+1}} \boldsymbol{F}_2(\boldsymbol{U}(t))\,\mathrm{d}t. \tag{2.3}$$

Here $\boldsymbol{F}_k(\boldsymbol{U}(t))$ represent the approximations of the physical fluxes $\boldsymbol{f}_k(\boldsymbol{u})$, $k = 1, 2$, on the cell interfaces. For the time integration of fluxes the midpoint rule is used. The intermediate values of the solution at cell interfaces are calculated by means of the approximate evolution operator $E_{\Delta t/2}$, which has been derived using the characteristics theory of hyperbolic systems, cf. Section 3. The approximate fluxes (e.g. on vertical edges) have the form

$$\boldsymbol{F}_k(\boldsymbol{U}^{n+\frac{1}{2}}) = \frac{1}{h}\int_0^h \boldsymbol{f}_k(E_{\Delta t/2} R_h \boldsymbol{U}^n)\,\mathrm{d}S_y, \quad k = 1, 2. \tag{2.4}$$

An analogous formula holds for horizontal edges. Here R_h is a recovery operator which transforms a piecewise constant function $\boldsymbol{U}$ to a piecewise bilinear function $R_h\boldsymbol{U}$, cf. Section 5.

If no recovery in (2.4) is used the whole method is of the first order. In this case we evaluate all space integrals exactly. For higher order schemes the interface integrals are approximated by a suitable numerical quadrature. We should also note that, if the interface integrals in the first order scheme are computed exactly, we actually compute the cell interface fluxes (2.4) in the following way:

$$\boldsymbol{F}_k(\boldsymbol{U}^{n+\frac{1}{2}}) = \boldsymbol{f}_k\left(\frac{1}{h}\int_0^h E_{\Delta t/2}\boldsymbol{U}^n\,\mathrm{d}S\right). \tag{2.5}$$

3. Linearized Euler equations and evolution operator

For better readability of the paper we have decided to present in this chapter a brief overview of the derivation of the exact evolution operator for the linearized Euler equations. Readers interested in more details of the calculations are referred to [17] or [10]. In order to derive an evolution operator for the Euler equations it is suitable to work with the system in primitive variables

$$\boldsymbol{v}_t + \boldsymbol{A}_1(\boldsymbol{v})\boldsymbol{v}_x + \boldsymbol{A}_2(\boldsymbol{v})\boldsymbol{v}_y = 0, \quad \boldsymbol{x} = (x, y)^T, \tag{3.1}$$

where $\boldsymbol{v} := (\varrho, u, v, p)^T$ is the vector of primitive variables and the Jacobian matrices $\boldsymbol{A}_1(\boldsymbol{v})$, $\boldsymbol{A}_2(\boldsymbol{v})$ are given by

$$\boldsymbol{A}_1(\boldsymbol{v}) := \begin{pmatrix} u & \varrho & 0 & 0 \\ 0 & u & 0 & \frac{1}{\varrho} \\ 0 & 0 & u & 0 \\ 0 & \gamma p & 0 & u \end{pmatrix}, \quad \boldsymbol{A}_2(\boldsymbol{v}) := \begin{pmatrix} v & 0 & \varrho & 0 \\ 0 & v & 0 & 0 \\ 0 & 0 & v & \frac{1}{\varrho} \\ 0 & 0 & \gamma p & v \end{pmatrix}.$$

Here ϱ denotes the density, u and v the components of velocity, p the pressure and γ the isentropic exponent; $\gamma = 1.4$ for dry air. In what follows we briefly describe the main technique for deriving an integral representation (or an exact evolution operator). First, we linearize the system (3.1) by freezing the Jacobian matrices at a suitable point $\tilde{P} = (\tilde{x}, \tilde{y}, \tilde{t})$. Denote by $\tilde{\boldsymbol{v}} = (\tilde{\varrho}, \tilde{u}, \tilde{v}, \tilde{p})$ the local variables at the point $\tilde{P}$ and by $\tilde{c}$ the local speed of sound there, i.e. $\tilde{c} = \sqrt{\gamma \tilde{p}/\tilde{\varrho}}$. Thus, the linearized system (3.1) with frozen constant coefficient matrices has the form

$$\boldsymbol{v}_t + \boldsymbol{A}_1(\tilde{\boldsymbol{v}})\boldsymbol{v}_x + \boldsymbol{A}_2(\tilde{\boldsymbol{v}})\boldsymbol{v}_y = 0, \quad \boldsymbol{x} = (x, y)^T. \tag{3.2}$$

The eigenvalues of the matrix pencil $\boldsymbol{A}(\tilde{\boldsymbol{v}}) = \boldsymbol{A}_1(\tilde{\boldsymbol{v}})n_x + \boldsymbol{A}_2(\tilde{\boldsymbol{v}})n_y$, where $\boldsymbol{n} = \boldsymbol{n}(\theta)$ $= (n_x, n_y)^T = (\cos\theta, \sin\theta)^T \in \mathbb{R}^2$ is a unit vector, are

$$\begin{aligned} \lambda_1 &= \tilde{u}\cos\theta + \tilde{v}\sin\theta - \tilde{c}, \\ \lambda_2 &= \lambda_3 = \tilde{u}\cos\theta + \tilde{v}\sin\theta, \\ \lambda_4 &= \tilde{u}\cos\theta + \tilde{v}\sin\theta + \tilde{c}, \end{aligned}$$

and the corresponding linearly independent right eigenvectors are

$$\begin{aligned} \boldsymbol{r}_1 &= \Big(-\frac{\tilde{\varrho}}{\tilde{c}}, \cos\theta, \sin\theta, -\tilde{\varrho}\tilde{c}\Big)^T, & \boldsymbol{r}_3 &= (0, \sin\theta, -\cos\theta, 0)^T, \\ \boldsymbol{r}_2 &= (1, 0, 0, 0)^T, & \boldsymbol{r}_4 &= \Big(\frac{\tilde{\varrho}}{\tilde{c}}, \cos\theta, \sin\theta, \tilde{\varrho}\tilde{c}\Big)^T. \end{aligned}$$

Let $\boldsymbol{R}(\tilde{\boldsymbol{v}})$ be the matrix of the right eigenvectors and $\boldsymbol{R}^{-1}(\tilde{\boldsymbol{v}})$ its inverse. Denote by $\boldsymbol{w}$ the vector of characteristic variables

$$\boldsymbol{w} = \boldsymbol{R}^{-1}(\tilde{\boldsymbol{v}})\boldsymbol{v} = \begin{pmatrix} \frac{1}{2}\Big(-\frac{p}{\tilde{\varrho}\tilde{c}} + u\cos\theta + v\sin\theta\Big) \\ \varrho - \frac{p}{\tilde{c}^2} \\ u\sin\theta - v\cos\theta \\ \frac{1}{2}\Big(\frac{p}{\tilde{\varrho}\tilde{c}} + u\cos\theta + v\sin\theta\Big) \end{pmatrix}.$$

Multiplying the system (3.2) by $\boldsymbol{R}^{-1}(\tilde{\boldsymbol{v}})$ from the left we obtain the following system written in characteristic variables:

$$\boldsymbol{w}_t + \boldsymbol{B}_1(\tilde{\boldsymbol{v}})\boldsymbol{w}_x + \boldsymbol{B}_2(\tilde{\boldsymbol{v}})\boldsymbol{w}_y = 0, \tag{3.3}$$

where $\boldsymbol{B}_k(\tilde{\boldsymbol{v}}) = \boldsymbol{R}^{-1}(\tilde{\boldsymbol{v}})\boldsymbol{A}_k(\tilde{\boldsymbol{v}})\boldsymbol{R}(\tilde{\boldsymbol{v}})$, $k = 1, 2$, are transformed Jacobian matrices.

Being in one space dimension the system (3.3) reduces to a diagonal system consisting of separated advection equations. Their exact evolution operator reads

$$w_l(x,t) = w_l(x - \lambda_l t, 0), \quad l = 1, \ldots, 4. \tag{3.4}$$

In the multi-dimensional case the system (3.3) will reduce to a diagonal one only if the Jacobian matrices $\boldsymbol{A}_1$, $\boldsymbol{A}_2$ commute, which is not the case of the two-dimensional Euler equations. Thus, we rewrite the system (3.3) in the form of the quasi-diagonalized system

$$\begin{aligned} &\boldsymbol{w}_t + \begin{pmatrix} \tilde{u} - \tilde{c}\cos\theta & 0 & 0 & 0 \\ 0 & \tilde{u} & 0 & 0 \\ 0 & 0 & \tilde{u} & 0 \\ 0 & 0 & 0 & \tilde{u} + \tilde{c}\cos\theta \end{pmatrix} \boldsymbol{w}_x \\ &\quad + \begin{pmatrix} \tilde{v} - \tilde{c}\sin\theta & 0 & 0 & 0 \\ 0 & \tilde{v} & 0 & 0 \\ 0 & 0 & \tilde{v} & 0 \\ 0 & 0 & 0 & \tilde{v} + \tilde{c}\sin\theta \end{pmatrix} \boldsymbol{w}_y = \boldsymbol{S} \end{aligned} \tag{3.5}$$

with

$$\boldsymbol{S} = \begin{pmatrix} \frac{1}{2}\tilde{c}\Big(\sin\theta\dfrac{\partial w_3}{\partial x} - \cos\theta\dfrac{\partial w_3}{\partial y}\Big) \\ 0 \\ \tilde{c}\sin\theta\Big(\dfrac{\partial w_1}{\partial x} - \dfrac{\partial w_4}{\partial x}\Big) - \tilde{c}\cos\theta\Big(\dfrac{\partial w_1}{\partial y} - \dfrac{\partial w_4}{\partial y}\Big) \\ \frac{1}{2}\tilde{c}\Big(-\sin\theta\dfrac{\partial w_3}{\partial x} + \cos\theta\dfrac{\partial w_3}{\partial y}\Big) \end{pmatrix}.$$

Each characteristic variable w_l, $l = 1, \ldots, 4$, is evolved in time along the corresponding bicharacteristic curve $\boldsymbol{x}_l$ defined by

$$\frac{\mathrm{d}\boldsymbol{x}_l}{\mathrm{d}t} = \boldsymbol{b}_{ll}(\boldsymbol{n}) := (b^1_{ll}, b^2_{ll})^T, \tag{3.6}$$

where $\boldsymbol{B}_1 = (b^1_{jk})_{j,k=1,\ldots,4}$, $\boldsymbol{B}_2 = (b^2_{jk})_{j,k=1,\ldots,4}$. The set of all bicharacteristics creates a mantle of the so-called Mach cone, see Fig. 1. In order to obtain the exact

evolution of each characteristic variable w_l we integrate the lth equation of the system (3.5) from the apex $P = (x, y, t+\Delta t)$ down to the corresponding footpoint $Q_l(\theta)$:

$$\begin{aligned} Q_1(\theta) &= (x - (\tilde{u} - \tilde{c}\cos\theta)\Delta t, y - (\tilde{v} - \tilde{c}\sin\theta)\Delta t, t), \\ Q_2 = Q_3 &= (x - \tilde{u}\Delta t, y - \tilde{v}\Delta t, t), \\ Q_4(\theta) &= (x - (\tilde{u} + \tilde{c}\cos\theta)\Delta t, y - (\tilde{v} + \tilde{c}\sin\theta)\Delta t, t). \end{aligned}$$

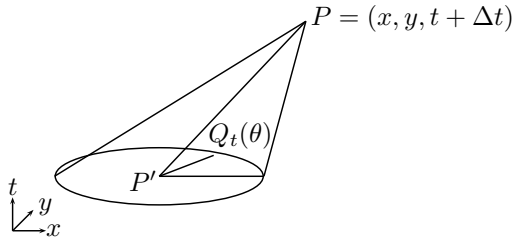

Figure 1. Bicharacteristics along the Mach cone through P and $Q_l(\theta)$.

Multiplying the resulting system from the left by the matrix $\boldsymbol{R}(\tilde{\boldsymbol{v}})$ yields the exact integral equations, i.e. the exact evolution operators, for the primitive variables of the linearized Euler equations (3.2):

$$\begin{aligned} (3.7)\quad \varrho(P) &= \varrho(Q_2) - \frac{p(Q_2)}{\tilde{c}^2} + \frac{1}{2\pi}\int_0^{2\pi}\Big[\frac{p(Q_1)}{\tilde{c}^2} \\ &\quad - \frac{\tilde{\varrho}}{\tilde{c}}u(Q_1)\cos\theta - \frac{\tilde{\varrho}}{\tilde{c}}v(Q_1)\sin\theta\Big]\,\mathrm{d}\theta - \frac{\tilde{\varrho}}{\tilde{c}}\frac{1}{2\pi}\int_0^{2\pi}\int_t^{t+\Delta t} S(\boldsymbol{\xi}, \tilde{t}, \theta)\,\mathrm{d}\tilde{t}\,\mathrm{d}\theta, \\ (3.8)\quad u(P) &= \frac{1}{2\pi}\int_0^{2\pi}\Big[-\frac{p(Q_1)}{\tilde{\varrho}\tilde{c}}\cos\theta + u(Q_1)\cos^2\theta + v(Q_1)\sin\theta\cos\theta\Big]\,\mathrm{d}\theta \\ &\quad + \frac{1}{2\pi}\int_0^{2\pi}\int_t^{t+\Delta t}\cos\theta S(\boldsymbol{\xi}, \tilde{t}, \theta)\,\mathrm{d}\tilde{t}\,\mathrm{d}\theta + \frac{1}{2}u(Q_2) \\ &\quad - \frac{1}{2\tilde{\varrho}}\int_t^{t+\Delta t} p_x(Q_2(\tilde{t}))\,\mathrm{d}\tilde{t}, \\ (3.9)\quad v(P) &= \frac{1}{2\pi}\int_0^{2\pi}\Big[-\frac{p(Q_1)}{\tilde{\varrho}\tilde{c}}\sin\theta + u(Q_1)\cos\theta\sin\theta + v(Q_1)\sin^2\theta\Big]\,\mathrm{d}\theta \\ &\quad + \frac{1}{2\pi}\int_0^{2\pi}\int_t^{t+\Delta t}\sin\theta S(\boldsymbol{\xi}, \tilde{t}, \theta)\,\mathrm{d}\tilde{t}\,\mathrm{d}\theta + \frac{1}{2}v(Q_2) \\ &\quad - \frac{1}{2\tilde{\varrho}}\int_t^{t+\Delta t} p_y(Q_2(\tilde{t}))\,\mathrm{d}\tilde{t}, \\ (3.10)\quad p(P) &= \frac{1}{2\pi}\int_0^{2\pi}[p(Q_1) - \tilde{\varrho}\tilde{c}u(Q_1)\cos\theta - \tilde{\varrho}\tilde{c}v(Q_1)\sin\theta]\,\mathrm{d}\theta \\ &\quad - \tilde{\varrho}\tilde{c}\frac{1}{2\pi}\int_0^{2\pi}\int_t^{t+\Delta t} S(\boldsymbol{\xi}, \tilde{t}, \theta)\,\mathrm{d}\tilde{t}\,\mathrm{d}\theta, \end{aligned}$$

where $\boldsymbol{\xi} = (x - (\tilde{u} - \tilde{c}\cos\theta)(t + \Delta t - \tilde{t}), y - (\tilde{v} - \tilde{c}\sin\theta)(t + \Delta t - \tilde{t}))$, and the so-called source term S is given in the form

$$S(\boldsymbol{x}, t, \theta) := \tilde{c}[u_x(\boldsymbol{x}, t, \theta)\sin^2\theta - (u_y(\boldsymbol{x}, t, \theta) + v_x(\boldsymbol{x}, t, \theta))\sin\theta\cos\theta + v_y(\boldsymbol{x}, t, \theta)\cos^2\theta].$$

4. Approximate evolution operators

The exact integral equations (3.7)–(3.10) for the solution to the linearized Euler equations (3.2) will be a basis for our further numerical approximations. The above exact integral representation (3.7)–(3.10) is implicit in time. In order to derive a numerical scheme which is explicit in time, the time integrals of the source terms, the so-called *mantle integrals*, have to be approximated with suitable numerical quadratures.

4.1. Approximate evolution operator EG3

As in [7] the integrals of the source term with respect to time will be approximated by the rectangle rule. Thus, we would need to evaluate derivatives of the velocity components at time t. However, it was proved in [7, Lemma 2.1] that the integrals of the source S can be simplified through integration by parts, which yields

$$\Delta t \int_0^{2\pi} S(t, \theta)\,\mathrm{d}\theta = \int_0^{2\pi} [u_Q\cos\theta + v_Q\sin\theta]\,\mathrm{d}\theta. \tag{4.1}$$

Analogously we can derive

$$\Delta t \int_0^{2\pi} S(t, \theta)\sin\theta\,\mathrm{d}\theta = \int_0^{2\pi} [2u_Q\sin\theta\cos\theta + v_Q(2\sin^2\theta - 1)]\,\mathrm{d}\theta \tag{4.2}$$

and

$$\Delta t \int_0^{2\pi} S(t, \theta)\cos\theta\,\mathrm{d}\theta = \int_0^{2\pi} [u_Q(2\cos^2\theta - 1) + 2v_Q\sin\theta\cos\theta]\,\mathrm{d}\theta. \tag{4.3}$$

Further, the integrals in (3.8) and (3.9) involving p_x and p_y need to be replaced by integrals over the cone mantle. This is done by using the Taylor expansion

$$p_x(P') = p_x(Q) + O(|P' - Q|) = p_x(Q) + O(\Delta t).$$

Then we use the rectangle rule in time and the Gauss theorem on a sonic circle $O = \{(x, y)\colon\ x^2 + y^2 \leqslant \tilde{c}^2 \Delta t^2\}$, which results in

$$
\begin{aligned}
(4.4) \qquad -\frac{1}{2\tilde{\varrho}} \int_t^{t+\Delta t} p_x(P'(\tilde{t}))\,\mathrm{d}\tilde{t} &= -\frac{\Delta t}{2\tilde{\varrho}} p_x(P') + O(\Delta t^2) \\
&= -\frac{1}{2\tilde{\varrho}\tilde{c}^2 \Delta t \pi} \int_O p_x(Q)\,\mathrm{d}x\,\mathrm{d}y + O(\Delta t^2) \\
&= -\frac{1}{2\tilde{\varrho}\tilde{c}^2 \Delta t \pi} \oint p(Q)\,\mathrm{d}y + O(\Delta t^2) \\
&= -\frac{1}{2\pi\tilde{\varrho}\tilde{c}} \int_0^{2\pi} p(Q)\cos\theta\,\mathrm{d}\theta + O(\Delta t^2).
\end{aligned}
$$

Analogously we derive the formula for p_y, which has the form

$$
-\frac{1}{2\tilde{\varrho}} \int_t^{t+\Delta t} p_y(P'(\tilde{t}))\,\mathrm{d}\tilde{t} = -\frac{1}{2\pi\tilde{\varrho}\tilde{c}} \int_0^{2\pi} p(Q)\sin\theta\,\mathrm{d}\theta.
$$

We have generated the approximate evolution operator for the Euler equations, which we call, analogously as for the wave equation in [7], the EG3 operator.

Approximate evolution operator EG3

$$
\begin{aligned}
(4.5) \quad \varrho(P) &= \varrho(Q_2) - \frac{p(Q_2)}{\tilde{c}^2} + \frac{1}{2\pi} \int_0^{2\pi} \left[\frac{p(Q_1)}{\tilde{c}^2} - 2\frac{\tilde{\varrho}}{\tilde{c}^2} \Big(u(Q_1)\cos\theta + v(Q_1)\sin\theta \Big) \right] \mathrm{d}\theta \\
&\quad + \mathcal{O}(\Delta t^2), \\
(4.6) \quad u(P) &= \frac{1}{2} u(Q_2) + \frac{1}{2\pi} \int_0^{2\pi} \Big[-\frac{p(Q_1)}{\tilde{\varrho}\tilde{c}} \cos\theta + u(Q_1)(3\cos^2\theta - 1) \\
&\qquad + 3v(Q_1)\sin\theta\cos\theta \Big] \mathrm{d}\theta + \mathcal{O}(\Delta t^2), \\
(4.7) \quad v(P) &= \frac{1}{2} v(Q_2) + \frac{1}{2\pi} \int_0^{2\pi} \Big[-\frac{p(Q_1)}{\bar{\varrho}\bar{c}} \sin\theta + 3u(Q_1)\sin\theta\cos\theta \\
&\qquad + v(Q_1)(3\sin^2\theta - 1) \Big] \mathrm{d}\theta + \mathcal{O}(\Delta t^2), \\
(4.8) \quad p(P) &= \frac{1}{2\pi} \int_0^{2\pi} [p(Q_1) - 2\tilde{\varrho}\tilde{c}(u(Q_1)\cos\theta + v(Q_1)\sin\theta)]\,\mathrm{d}\theta + \mathcal{O}(\Delta t^2).
\end{aligned}
$$

Note that other integral rules for the time approximation of the source terms can be used as well. They would lead to the approximate evolution operators EG1, EG2 and EG4. The notation is used in analogy to [7], [18]. We decided to present here only the operator EG3, which yields the most accurate numerical approximation among EG1–EG4.

On the other hand, the above FVEG methods suffered from the restrictive stability limits. For example, for the FVEG3 scheme a typical CFL stability limit was 0.63 and 0.56 for first and second order schemes, respectively. The CFL number is defined as CFL $= \max\{|u| + c, |v| + c\}\Delta t/h$. Note that integrals around the sonic circle, i.e. $\int_0^{2\pi} \mathrm{d}\theta$, are evaluated for piecewise constant or piecewise bilinear data exactly. Therefore, obviously, the only step where the stability could be reduced was the time approximation of the mantle integral. For example, in the first order EG scheme we work with piecewise constant data, in which case a discontinuity cuts through the cone mantle. Naturally, classical quadratures, such as the rectangle or the trapezoidal rule, which were used for the EG1–EG4 schemes, cannot correctly reproduce integration of discontinuous data.

4.2. Approximate evolution operator EG5

Since the approximate evolution operators EG1–EG4 did not provide full stability up to the CFL number 1, more appropriate numerical quadratures for time integration along the mantle of the Mach cone have been constructed in [9]. For the one-dimensional advection equation it is known that any scheme which is stable up to CFL $= 1$ has to reproduce the exact solution at CFL $= 1$. In [9] the following design principle was proposed for the wave equation system. Consider plane wave data which are parallel to one of the spatial axis. For a first order scheme these are taken to be piecewise constant, i.e. one-dimensional Riemann data in x- or y-directions. Now we look for approximate evolution operators that reproduce the exact solution at the the apex of the bicharacteristic cone centered at the original discontinuity. When considering slopes for second order schemes we derive approximate evolution operators for the slopes that again reproduce the solution for continuous piecewise linear data exactly at the apex of the bicharacteristic cone centered at the kink of such data.

In the dissertation of the second author [17] the rigorous derivation of the approximate evolution operator for the Euler equations using the above design principles has been done. We have decided not to present these rather lengthy calculations here, since it would enlarge the size of the paper substantially. Instead we only present the formulations of the approximate evolution operator EG5 for both piecewise constant and piecewise bilinear data. Numerical experiments presented in [9], [12], [17] demonstrate that the FVEG5 method is approximately three times more accurate than the FVEG3 method and has the CFL limit close to 1. Theoretical error analysis of the FVEG5 scheme for linear and linearized systems has been done in [17].

Approximate evolution operator E_Δ^{const} for *piecewise constant* data

$$\varrho(P) = \varrho(Q_2) - \frac{p(Q_2)}{\tilde{c}^2} + \frac{1}{2\pi}\int_0^{2\pi}\Big[\frac{p(Q_1)}{\tilde{c}^2} - \frac{\tilde{\varrho}}{\tilde{c}}u(Q_1)\operatorname{sgn}(\cos\theta) - \frac{\tilde{\varrho}}{\tilde{c}}v(Q_1)\operatorname{sgn}(\sin\theta)\Big]\,\mathrm{d}\theta, \tag{4.9}$$

$$u(P) = \frac{1}{2\pi}\int_0^{2\pi}\Big[-\frac{p(Q_1)}{\tilde{\varrho}\tilde{c}}\operatorname{sgn}(\cos\theta) + u(Q_1)\Big(\frac{1}{2}+\cos^2\theta\Big) + v(Q_1)\sin\theta\cos\theta\Big]\,\mathrm{d}\theta, \tag{4.10}$$

$$v(P) = \frac{1}{2\pi}\int_0^{2\pi}\Big[-\frac{p(Q_1)}{\tilde{\varrho}\tilde{c}}\operatorname{sgn}(\sin\theta) + u(Q_1)\cos\theta\sin\theta + v(Q_1)\Big(\frac{1}{2}+\sin^2\theta\Big)\Big]\,\mathrm{d}\theta, \tag{4.11}$$

$$p(P) = \frac{1}{2\pi}\int_0^{2\pi}[p(Q_1) - \tilde{\varrho}\tilde{c}u(Q_1)\operatorname{sgn}(\cos\theta) - \tilde{\varrho}\tilde{c}v(Q_1)\operatorname{sgn}(\sin\theta)]\,\mathrm{d}\theta. \tag{4.12}$$

Approximate evolution operator E_Δ^{bilin} for *piecewise bilinear* data

$$\varrho(P) = \varrho(Q_2) + \frac{1}{4}\int_0^{2\pi}\frac{1}{\tilde{c}^2}[p(Q_1)-p(Q_2)]\,\mathrm{d}\theta - \frac{1}{\pi}\int_0^{2\pi}\frac{\tilde{\varrho}}{\tilde{c}}[u(Q_1)\cos\theta + v(Q_1)\sin\theta]\,\mathrm{d}\theta + \mathcal{O}(\Delta t^2), \tag{4.13}$$

$$u(P) = u(Q_2) - \frac{1}{\pi}\int_0^{2\pi}\frac{p(Q_1)}{\tilde{\varrho}\tilde{c}}\cos\theta\,\mathrm{d}\theta + \frac{1}{4}\int_0^{2\pi}\Big[3(u(Q_1)\cos\theta + v(Q_1)\sin\theta)\cos\theta - u(Q_1)\frac{1}{2}u(Q_2)\Big]\,\mathrm{d}\theta + \mathcal{O}(\Delta t^2), \tag{4.14}$$

$$v(P) = v(Q_2) - \frac{1}{\pi}\int_0^{2\pi}\frac{p(Q_1)}{\bar{\varrho}\bar{a}}\sin\theta\,\mathrm{d}\theta + \frac{1}{4}\int_0^{2\pi}\Big[3(u(Q_1)\cos\theta + v(Q_1)\sin\theta)\sin\theta - v(Q_1) - \frac{1}{2}v(Q_2)\Big]\,\mathrm{d}\theta + \mathcal{O}(\Delta t^2), \tag{4.15}$$

$$p(P) = p(Q_2) + \frac{1}{4}\int_0^{2\pi}[p(Q_1)-p(Q_2)]\,\mathrm{d}\theta - \frac{1}{\pi}\int_0^{2\pi}\tilde{\varrho}\tilde{c}[u(Q_1)\cos\theta + v(Q_1)\sin\theta]\,\mathrm{d}\theta + \mathcal{O}(\Delta t^2). \tag{4.16}$$

5. Second order schemes

In the first order schemes no reconstruction is used and the exact solution $\boldsymbol{u}(x, y, t_n)$ is approximated by the piecewise constant function $\boldsymbol{U}^n$. The integrals along the Mach cone and over each cell interface are computed exactly, i.e. no approximation is used. If we want to obtain higher order finite volume EG schemes, we have to replace the piecewise constant function $\boldsymbol{U}^n$ by a higher degree polynomial. One possibility to obtain the second order scheme is to apply on each mesh cell Ω_{ij}, $i, j \in \mathbb{Z}$ the discontinuous bilinear recovery

$$R_h^D \boldsymbol{U}^n\big|_{\Omega_{ij}} = \Big(1+\frac{(x-x_i)}{h}\mu_x\mu_y^2\delta_x+\frac{(y-y_j)}{h}\mu_x^2\mu_y\delta_y+\frac{(x-x_i)(y-y_j)}{h^2}\mu_x\mu_y\delta_x\delta_y\Big)\boldsymbol{U}_{ij}^n,$$

where $\mu_x v(x) = \frac{1}{2}\big(v\big(x+\frac{1}{2}h\big) + v\big(x-\frac{1}{2}h\big)\big)$, $\delta_x v(x) = v\big(x+\frac{1}{2}h\big) - v\big(x-\frac{1}{2}h\big)$, an analogous notation being used for y-direction. Note that this bilinear recovery is constructed in such a way that it is conservative, i.e.

$$\frac{1}{h^2}\int_{\Omega_{ij}} R_h\boldsymbol{U}^n \,\mathrm{d}x\,\mathrm{d}y = \frac{1}{h^2}\int_{\Omega_{ij}} \boldsymbol{U}^n \,\mathrm{d}x\,\mathrm{d}y.$$

Another possibility is to use continuous but non-conservative bilinear recovery. In this case we have on each mesh cell

$$R_h^C \boldsymbol{U}^n\big|_{\Omega_{ij}} = \Big(\mu_x^2\mu_y^2 + \frac{(x-x_i)}{h}\mu_x\mu_y^2\delta_x + \frac{(y-y_j)}{h}\mu_x^2\mu_y\delta_y + \frac{(x-x_i)(y-y_j)}{h^2}\mu_x\mu_y\delta_x\delta_y\Big)\boldsymbol{U}_{ij}^n. \tag{5.1}$$

In our numerical experiments we have used the conservative bilinear recovery R_h^D for the FVEG1–FVEG4 schemes. The second order FVEG5 scheme is constructed as a combination of the approximate evolution operator $E_\Delta^{\mathrm{bilin}}$ which evolves the continuous bilinear data, and the approximate evolution operator $E_\Delta^{\mathrm{const}}$ which corrects the evolution of the constant part in order to preserve conservativity of the cell interface values $\boldsymbol{U}^{n+\frac{1}{2}}$, cf. also [9]. Thus for the FVEG5 scheme we use the formula

$$\boldsymbol{U}^{n+\frac{1}{2}} = E_\Delta^{\mathrm{const}}(1-\mu_x^2\mu_y^2)\boldsymbol{U}^n + E_\Delta^{\mathrm{bilin}} R_h^C \boldsymbol{U}^n.$$

It is a well-known fact that higher order methods can suffer from oscillations near discontinuities. In order to avoid developing oscillations in the solution we control gradients of the recovered functions by a limiter. There are many possibilities to choose a suitable limiter. In our numerical computations we have used the so-called minmod limiter, see [5], [17].

As we have mentioned above, in the second order scheme we compute exactly only the Mach cone integrals. Integrals over cell interfaces are computed by some suitable numerical quadratures. In the next subsection we study the L^1-stability for these quadrature rules.

5.1. L^1-stability analysis of the cell interface flux integrals

Natural quadrature points on cell interface are vertices used for the trapezoidal rule and midpoints used in the midpoint rule. Combining vertices and midpoints yields Simpson's rule. In what follows we consider these three quadrature rules for approximation of the cell interface integrals.

Let us consider a scalar linear advection equation in two-dimensions

$$U_t + \tilde{u}U_x + \tilde{v}U_y = 0, \tag{5.2}$$

where $\tilde{u}, \tilde{v} > 0$ are positive constant velocities. We can write the finite volume scheme for the equation (5.2) as

$$h^2(U_{ij}^{n+1} - U_{ij}^n) + h\Delta t\Big(F_{i+\frac{1}{2}j}^{n+\frac{1}{2}} - F_{i-\frac{1}{2}j}^{n+\frac{1}{2}} + G_{ij+\frac{1}{2}}^{n+\frac{1}{2}} - G_{ij-\frac{1}{2}}^{n+\frac{1}{2}}\Big) = 0, \tag{5.3}$$

where $h > 0$ is the mesh size parameter. The exact evaluation of the fluxes at time $t_{n+\frac{1}{2}} = t_n + \frac{1}{2}\Delta t$ gives

$$\begin{aligned} F_{i+\frac{1}{2}j}^{n+\frac{1}{2}} &= \tilde{u}\left[\frac{(\tilde{u}\Delta th - \frac{1}{2}\tilde{u}\tilde{v}\Delta t^2)U_{ij}^n + \frac{1}{2}\tilde{u}\tilde{v}\Delta t^2 U_{i-1j}^n}{\tilde{u}\Delta th}\right] \\ &= \tilde{u}\left[\Big(1 - \frac{\tilde{v}\Delta t}{2h}\Big)U_{ij}^n + \frac{\tilde{v}\Delta t}{2h}U_{i-1j}^n\right], \end{aligned} \tag{5.4}$$

$$F_{i-\frac{1}{2}j}^{n+\frac{1}{2}} = \tilde{u}\left[\Big(1 - \frac{\tilde{v}\Delta t}{2h}\Big)U_{i-1j}^n + \frac{\tilde{v}\Delta t}{2h}U_{i-1j-1}^n\right], \tag{5.5}$$

$$G_{ij+\frac{1}{2}}^{n+\frac{1}{2}} = \tilde{v}\left[\Big(1 - \frac{\tilde{u}\Delta t}{2h}\Big)U_{ij}^n + \frac{\tilde{u}\Delta t}{2h}U_{ij-1}^n\right], \tag{5.6}$$

$$G_{ij-\frac{1}{2}}^{n+\frac{1}{2}} = \tilde{v}\left[\Big(1 - \frac{\tilde{u}\Delta t}{2h}\Big)U_{ij-1}^n + \frac{\tilde{u}\Delta t}{2h}U_{i-1j-1}^n\right]. \tag{5.7}$$

Then the finite volume scheme (5.3) becomes

$$\begin{aligned} U_{ij}^{n+1} &= U_{ij}^n - \Big[\frac{\tilde{u}\Delta t}{h}\Delta_x - \frac{\tilde{u}\tilde{v}\Delta t^2}{2h^2}\Delta_x\Delta_y\Big]U_{ij}^n \\ &\quad - \Big[\frac{\tilde{v}\Delta t}{h}\Delta_y - \frac{\tilde{u}\tilde{v}\Delta t^2}{2h^2}\Delta_x\Delta_y\Big]U_{ij}^n \\ &= \Big[1 - \frac{\tilde{u}\Delta t}{h}\Delta_x\Big]\Big[1 - \frac{\tilde{v}\Delta t}{h}\Delta_y\Big]U_{ij}^n, \end{aligned} \tag{5.8}$$

where $\Delta_x U_{ij}$, $\Delta_y U_{ij}$, are the backward differences in x-, y-direction, respectively, i.e. e.g. $\Delta_x U_{ij} = U_{ij} - U_{i-1j}$. This scheme is a tensor product of the one-dimensional upwind schemes and it is well-known that it is monotone and stable up to CFL $\leqslant 1$, where we define CFL $:= \max\{\tilde{u}\Delta t/h, \tilde{v}\Delta t/h\}$. More precisely, under the above CFL condition let us show the L^1-stability of the scheme, i.e. $\|U^{n+1}\|_1 \leqslant \|U^n\|_1$. For the discrete grid function U^n we define the discrete L^1-norm by

$$\|U^n\|_1 = h^2 \sum_{i,j\in\mathbb{Z}} |U^n_{ij}|. \tag{5.9}$$

We can rewrite equation (5.8) as

$$\begin{aligned} U^{n+1}_{ij} = {} & \Big(1 - \frac{\tilde{u}\Delta t}{h}\Big)\Big(1 - \frac{\tilde{v}\Delta t}{h}\Big)U^n_{ij} + \frac{\tilde{v}\Delta t}{h}\Big(1 - \frac{\tilde{u}\Delta t}{h}\Big)U^n_{ij-1} \\ & + \frac{\tilde{u}\Delta t}{h}\Big(1 - \frac{\tilde{v}\Delta t}{h}\Big)U^n_{i-1j} + \frac{\tilde{u}\tilde{v}\Delta t^2}{h^2}U^n_{i-1j-1}. \end{aligned}$$

From the definition of the L^1-norm we have

$$\begin{aligned} \|U^{n+1}\|_1 &= h^2 \sum_{i,j} |U^{n+1}_{ij}| \\ &\leqslant h\Big[\sum_{i,j}\Big|\Big(1 - \frac{\tilde{u}\Delta t}{h}\Big)\Big(1 - \frac{\tilde{v}\Delta t}{h}\Big)U^n_{ij}\Big| + \sum_{i,j}\Big|\frac{\tilde{v}\Delta t}{h}\Big(1 - \frac{\tilde{u}\Delta t}{h}\Big)U^n_{ij-1}\Big| \\ &\quad + \sum_{i,j}\Big|\frac{\tilde{u}\Delta t}{h}\Big(1 - \frac{\tilde{v}\Delta t}{h}\Big)U^n_{i-1j}\Big| + \sum_{i,j}\Big|\frac{\tilde{u}\tilde{v}\Delta t^2}{h^2}U^n_{i-1j-1}\Big|\Big]. \end{aligned}$$

Thus, if the conditions

$$\begin{aligned} &\Big(1 - \frac{\tilde{u}\Delta t}{h}\Big)\Big(1 - \frac{\tilde{v}\Delta t}{h}\Big) \geqslant 0, \qquad \frac{\tilde{v}\Delta t}{h}\Big(1 - \frac{\tilde{u}\Delta t}{h}\Big) \geqslant 0, \\ &\frac{\tilde{u}\Delta t}{h}\Big(1 - \frac{\tilde{v}\Delta t}{h}\Big) \geqslant 0, \qquad \frac{\tilde{u}\tilde{v}\Delta t^2}{h^2} \geqslant 0 \end{aligned} \tag{5.10}$$

hold then the scheme (5.8) is stable, since we can take terms from (5.10) in front of the absolute value. We get

$$\begin{aligned} \|U^{n+1}\|_1 &\leqslant h^2\Big[\Big(1 - \frac{\tilde{u}\Delta t}{h}\Big)\Big(1 - \frac{\tilde{v}\Delta t}{h}\Big)\sum_{i,j}|U^n_{ij}| + \frac{\tilde{v}\Delta t}{h}\Big(1 - \frac{\tilde{u}\Delta t}{h}\Big)\sum_{i,j}|U^n_{ij-1}| \\ &\quad + \frac{\tilde{u}\Delta t}{h}\Big(1 - \frac{\tilde{v}\Delta t}{h}\Big)\sum_{i,j}|U^n_{i-1j}| + \frac{\tilde{u}\tilde{v}\Delta t^2}{h^2}\sum_{i,j}|U^n_{i-1j-1}|\Big] \\ &= \Big(1 - \frac{\tilde{u}\Delta t}{h}\Big)\Big(1 - \frac{\tilde{v}\Delta t}{h}\Big)\|U^n\|_1 + \frac{\tilde{v}\Delta t}{h}\Big(1 - \frac{\tilde{u}\Delta t}{h}\Big)\|U^n\|_1 \\ &\quad + \frac{\tilde{u}\Delta t}{h}\Big(1 - \frac{\tilde{v}\Delta t}{h}\Big)\|U^n\|_1 + \frac{\tilde{u}\tilde{v}\Delta t^2}{h^2}\|U^n\|_1 = \|U^n\|_1. \end{aligned}$$

Note that conditions (5.10) can be rewritten in the form

$$0 \leqslant \frac{\tilde{u}\Delta t}{h} \leqslant 1 \quad \text{and} \quad 0 \leqslant \frac{\tilde{v}\Delta t}{h} \leqslant 1,$$

which corresponds to the CFL condition given above.

Now we would like to find stability conditions for the trapezoidal rule approximation of the interface integrals of fluxes. If we replace the exact fluxes (5.4)–(5.7) by the *trapezoidal rule*, we get

$$F^{n+\frac{1}{2}}_{i+\frac{1}{2}j} = \frac{\tilde{u}}{2}(U^n_{ij} + U^n_{ij-1}), \qquad F^{n+\frac{1}{2}}_{i-\frac{1}{2}j} = \frac{\tilde{u}}{2}(U^n_{i-1j} + U^n_{i-1j-1}),$$
$$G^{n+\frac{1}{2}}_{ij+\frac{1}{2}} = \frac{\tilde{v}}{2}(U^n_{ij} + U^n_{i-1j}), \qquad G^{n+\frac{1}{2}}_{ij-\frac{1}{2}} = \frac{\tilde{v}}{2}(U^n_{ij-1} + U^n_{i-1j-1}).$$

Then the finite volume scheme (5.3) has the form

$$\begin{aligned} U^{n+1}_{ij} &= U^n_{ij} - \frac{\tilde{u}\Delta t}{2h}[\Delta_x + \Delta_x - \Delta_x\Delta_y]U^n_{ij} \\ &\quad - \frac{\tilde{v}\Delta t}{2h}[\Delta_y + \Delta_y - \Delta_x\Delta_y]U^n_{ij} \\ &= \Big[1 - \frac{\tilde{u}\Delta t}{h}\Delta_x\Big]\Big[1 - \frac{\tilde{v}\Delta t}{h}\Delta_y\Big]U^n_{ij} \\ &\quad + \Big(\frac{\tilde{u}\Delta t}{2h} - \frac{\tilde{u}\tilde{v}\Delta t^2}{h^2} + \frac{\tilde{v}\Delta t}{2h}\Big)\Delta_x\Delta_y U^n_{ij}. \end{aligned} \tag{5.11}$$

Let us show that this scheme is stable only if $\tilde{u}\Delta t/h = \tilde{v}\Delta t/h$. We can rewrite (5.11) as

$$\begin{aligned} U^{n+1}_{ij} &= \frac{1}{2}\Big(2 - \frac{\tilde{u}\Delta t}{h} - \frac{\tilde{v}\Delta t}{h}\Big)U^n_{ij} + \frac{1}{2}\Big(-\frac{\tilde{u}\Delta t}{h} + \frac{\tilde{v}\Delta t}{h}\Big)U^n_{ij-1} \\ &\quad + \frac{1}{2}\Big(\frac{\tilde{u}\Delta t}{h} - \frac{\tilde{v}\Delta t}{h}\Big)U^n_{i-1j} + \frac{1}{2}\Big(\frac{\tilde{u}\Delta t}{h} + \frac{\tilde{v}\Delta t}{h}\Big)U^n_{i-1j-1} \end{aligned}$$

and hence the L^1-norm can be bounded from above in the following way:

$$\begin{aligned} \|U^{n+1}\|_1 &= h^2 \sum_{i,j} |U^{n+1}_{ij}| \\ &\leqslant \frac{h^2}{2}\Big[\sum_{i,j}\Big|\Big(2 - \frac{\tilde{u}\Delta t}{h} - \frac{\tilde{v}\Delta t}{h}\Big)U^n_{ij}\Big| + \sum_{i,j}\Big|\Big(-\frac{\tilde{u}\Delta t}{h} + \frac{\tilde{v}\Delta t}{h}\Big)U^n_{ij-1}\Big| \\ &\quad + \sum_{i,j}\Big|\Big(\frac{\tilde{u}\Delta t}{h} - \frac{\tilde{v}\Delta t}{h}\Big)U^n_{i-1j}\Big| + \sum_{i,j}\Big|\Big(\frac{\tilde{u}\Delta t}{h} + \frac{\tilde{v}\Delta t}{h}\Big)U^n_{i-1j-1}\Big|\Big]. \end{aligned} \tag{5.12}$$

In order to obtain stability of the scheme the following four conditions have to hold simultaneously:

$$\frac{\tilde{u}\Delta t}{h} + \frac{\tilde{v}\Delta t}{h} \leqslant 2, \qquad \frac{\tilde{u}\Delta t}{h} - \frac{\tilde{v}\Delta t}{h} \leqslant 0,$$
$$\frac{\tilde{u}\Delta t}{h} - \frac{\tilde{v}\Delta t}{h} \geqslant 0, \qquad \frac{\tilde{u}\Delta t}{h} + \frac{\tilde{v}\Delta t}{h} \geqslant 0.$$

Thus we need to require that $\tilde{u}\Delta t/h = \tilde{v}\Delta t/h$, $\tilde{u}\Delta t/h \leqslant 1$ and $\tilde{v}\Delta t/h \leqslant 1$. If we put these conditions into (5.12), we obtain

$$\begin{aligned}\|U^{n+1}\|_1 &\leqslant \frac{h^2}{2}\Bigg[\Big(2 - \frac{\tilde{u}\Delta t}{h} - \frac{\tilde{v}\Delta t}{h}\Big)\sum_{i,j}|U^n_{ij}| + \Big(-\frac{\tilde{u}\Delta t}{h} + \frac{\tilde{v}\Delta t}{h}\Big)\sum_{i,j}|U^n_{ij-1}| \\ &\quad + \Big(\frac{\tilde{u}\Delta t}{h} - \frac{\tilde{v}\Delta t}{h}\Big)\sum_{i,j}|U^n_{i-1j}| + \Big(\frac{\tilde{u}\Delta t}{h} + \frac{\tilde{v}\Delta t}{h}\Big)\sum_{i,j}|U^n_{i-1j-1}|\Bigg] \\ &= \frac{1}{2}\Bigg[\Big(2 - 2\frac{\tilde{u}\Delta t}{h}\Big)\|U^n\|_1 + \Big(2\frac{\tilde{u}\Delta t}{h}\Big)\|U^n\|_1\Bigg] = \|U^n\|_1.\end{aligned}$$

We have shown that the trapezoidal rule yields a stable finite volume scheme only if $\tilde{u} = \tilde{v}$ and hence it is suited only for special situations, e.g. for the approximation of edge integrals for the wave equation without advection, i.e. $\tilde{u} = 0 = \tilde{v}$. For other systems with arbitrary advections, such as the Euler equations, this quadrature rule yields an unstable scheme.

In an analogous way we can derive a stability condition for the FV scheme using the *midpoint rule* for flux integrals, which reads

$$\frac{\tilde{u}\Delta t}{h} + \frac{\tilde{v}\Delta t}{h} \leqslant 1, \quad 0 \leqslant \frac{\tilde{u}\Delta t}{h}, \quad 0 \leqslant \frac{\tilde{v}\Delta t}{h}.$$

If *Simpson's rule* is used the following stability conditions have to be satisfied:

$$\frac{1}{5}\frac{\tilde{v}\Delta t}{h} \leqslant \frac{\tilde{u}\Delta t}{h} \leqslant 5\frac{\tilde{v}\Delta t}{h} \quad \text{and} \quad 0 \leqslant \frac{\tilde{u}\Delta t}{h} + \frac{\tilde{v}\Delta t}{h} \leqslant \frac{6}{5}.$$

This analysis yields the conclusion that for problems with arbitrary advection velocities $\tilde{u}$, $\tilde{v}$ Simpson's rule leads in general to the most stable discretization of the flux integrals. It is the numerical quadrature that we use in our numerical experiments in Section 6. Note that this L^1-stability analysis holds for general two-dimensional FV schemes.

6. Numerical experiments

In this section, through numerical simulations, we illustrate the performance of the FVEG methods for the linear wave equation system and for fully nonlinear Euler equations of gas dynamics.

6.1. Water waves propagation

It is known that the approximation of circular waves on rectangular meshes can cause difficulties. Particularly, if the dimensional splitting approach is used, spurious mesh oriented structures can be developed, see e.g. [5], [7], [14] and the references therein.

We consider the wave equation system

$$\boldsymbol{v}_t + \boldsymbol{A}_1(\boldsymbol{v})\boldsymbol{v}_x + \boldsymbol{A}_2(\boldsymbol{v})\boldsymbol{v}_y = 0, \quad \boldsymbol{x} = (x, y)^T, \tag{6.1}$$

where $\boldsymbol{v} := (\varphi, u, v)^T$. Here φ is the pressure wave, u and v are the velocities in x-, y-direction, respectively. The Jacobian matrices $\boldsymbol{A}_1(\boldsymbol{v})$, $\boldsymbol{A}_2(\boldsymbol{v})$ are given by

$$\boldsymbol{A}_1(\boldsymbol{v}) := \begin{pmatrix} 0 & c & 0 \\ c & 0 & 0 \\ 0 & 0 & 0 \end{pmatrix}, \quad \boldsymbol{A}_2(\boldsymbol{v}) := \begin{pmatrix} 0 & 0 & c \\ 0 & 0 & 0 \\ c & 0 & 0 \end{pmatrix},$$

where c is a sound speed; see [9] for approximate evolution operators of (6.1). Consider the following initial data modeling a pointwise disturbance:

$$\begin{aligned} \varphi(\boldsymbol{x}, 0) &= -c\exp(-15x^2 - 15y^2), \\ u(\boldsymbol{x}, 0) &= 0 = v(\boldsymbol{x}, 0). \end{aligned}$$

The computational domain $[-3, 3] \times [-3, 3]$ is divided into 100×100 cells. The first component φ of the solution obtained by the second order FVEG scheme at different times from $T = 0.2$ until $T = 8.0$ is shown in Fig. 2. We can notice a well resolved symmetric circular wave. As time evolves the wave propagates and is being reflected from the left boundary. The Mach stem which is evolving behind the main wave can be recognized at time $t = 8.0$. This problem can be considered as a model for a pointwise disturbance of water surface, e.g. as it occurs when a stone is thrown into a lake.

As mentioned above, we set reflected boundary conditions on the left vertical boundary and absorbing boundary conditions elsewhere. In numerical experiments presented in this paper we have implemented absorbing boundary conditions by linear extrapolation of all quantities to the so-called ghost cells, which are adjacent

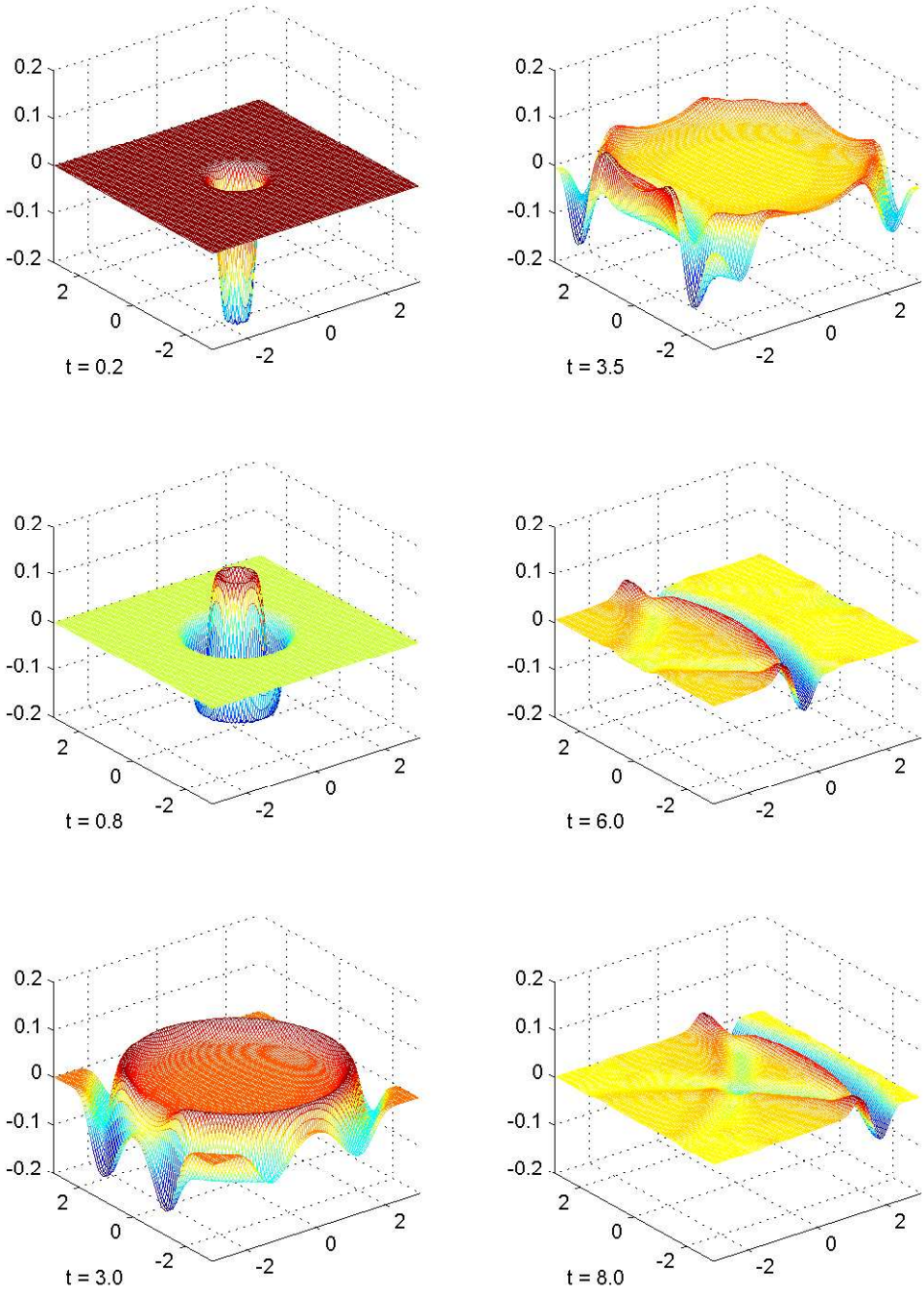

Figure 2. Propagation of circular water wave.

to the boundary of the computational domain. Thus we have, e.g. for the pressure wave φ,

$$\varphi_{-1j} = \varphi_{0j}, \;\; \varphi_{-2j} = \varphi_{1j}, \quad j \in \mathbb{Z},$$

where Ω_{-1j}, Ω_{-2j} and Ω_{0j}, Ω_{1j} are the ghost cells and the cells belonging to Ω, respectively.

Note that due to the second order method two layers of the ghost cells are needed. The reflected boundary conditions are easily modelled by reflecting the interior data across the boundary and negating the normal component of velocity. Thus we have on the left vertical boundary

$$u_{-1j} = -u_{0j}, \;\; u_{-2j} = -u_{1j}, \quad j \in \mathbb{Z}.$$

Other quantities, i.e. φ, v, are extrapolated.

6.2. Interaction between circular shocks and reflected waves

In this example we consider again the wave equation system (6.1) with discontinuous initial data

$$\begin{aligned} &\varphi = 1, \quad u = 0, \quad v = 0, \quad \|\boldsymbol{x}\| < 0.4, \\ &\varphi = 0, \quad u = 0, \quad v = 0, \quad \text{elsewhere.} \end{aligned}$$

The computational domain $[-1,1] \times [-1,1]$ is divided into 200×200 cells. We implemented reflected boundary conditions on the vertical boundaries and absorbing boundary conditions on the horizontal ones. In Fig. 3 the pressure wave distribution at different times $T = 0.3$, 1.0, 1.3 is depicted. We can notice a well-resolved circular shock traveling away from the center of the computational domain. As time evolves the shock reaches the vertical boundaries and is reflected into the computational domain. Due to the linear model, interactions between the linear circular shock and the reflected waves can be observed very well.

6.3. Static disc problem for the Euler equations

This is a two-dimensional problem with circular symmetry. We consider nonlinear hyperbolic systems of Euler equations (3.1). The computational domain is $[-1,1] \times [-1,1]$ and the boundary conditions are periodical. Here the initial conditions are

$$\begin{aligned} \varrho(x,y,0) &= \begin{cases} 3, & \text{if } (x^2+y^2) \leqslant 0.5, \\ 1, & \text{otherwise,} \end{cases} \\ u(x,y,0) &= 0, \\ v(x,y,0) &= 0, \\ p(x,y,0) &= 1. \end{aligned}$$

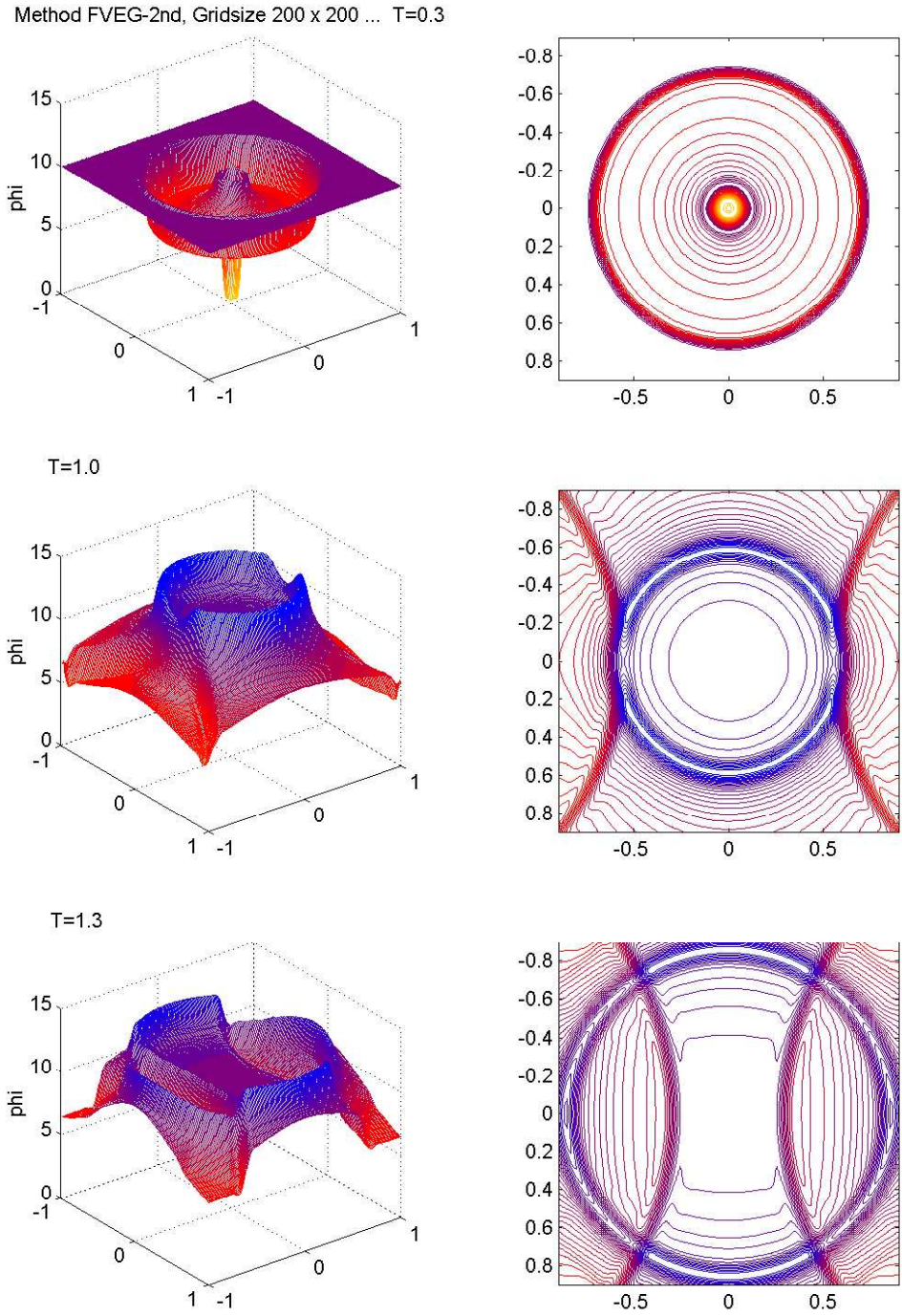

Figure 3. Interaction between the circular shock and reflected waves.

Thus we have contact discontinuity along the disc boundary. The exact solution is the same as the initial condition, i.e. disc with radius 0.5. We compute this problem up to time $t = 10$ on different meshes (16×16, 32×32, 64×64, 128×128). The initial conditions for cells lying on the boundary of the circular disc are implemented by approximate weighted integral averages of initial data. In Fig. 4 we show isolines of density computed on different meshes by the second order finite volume schemes EG3 and EG5. In the middle column the weighted initial data which we used are plotted. This example demonstrates that the steady contact discontinuity is resolved in a correct way preserving the multi-dimensional phenomena as well. Note that Kröger and Noelle reported in [3] that their MoT-ICE method fails for this example producing a totally incorrect resolution as we can see in Tab. 1. We present the L^1-error in the ϱ component for the finite volume EG3 and EG5 schemes and for the MoT-ICE scheme on different meshes.

mesh	EG3	EG5	MoT − ICE
16	0	0	$7.1795 \cdot 10^{-1}$
32	$0.4 \cdot 10^{-11}$	$0.2 \cdot 10^{-11}$	$5.1174 \cdot 10^{-1}$
64	$1.2 \cdot 10^{-11}$	$1.2 \cdot 10^{-11}$	$3.8264 \cdot 10^{-1}$

Table 1. L^1-error in the ϱ component for static disk problem (with periodic boundary conditions).

References

[1] *M. Brio, A. R. Zakharian, and G. M. Webb*: Two-dimensional Riemann solver for Euler equations of gas dynamics. J. Comput. Phys. *167* (2001), 177–195. Zbl 1043.76042

[2] *M. Fey*: Multidimensional upwinding, Part II. Decomposition of the Euler equations into advection equations. J. Comput. Phys. *143* (1998), 181–199. Zbl 0932.76051

[3] *T. Kröger, S. Noelle*: Numerical comparison of the Method of Transport to a standard scheme. Comput. Fluids *34* (2003), 541–560. Zbl 1077.35007

[4] *A. Kurganov, S. Noelle, and G. Petrova*: Semidiscrete central-unpwind schemes for hyperbolic conservation laws and Hamilton-Jacobi equations. SIAM J. Sci. Comput. *23* (2001), 707–740. Zbl 0998.65091

[5] *R. J. LeVeque*: Wave propagation algorithms for multidimensional hyperbolic systems. J. Comput. Phys. *131* (1997), 327–353. Zbl 0872.76075

[6] *J. Li, M. Lukáčová-Medviďová, G. Warnecke*: Evolution Galerkin schemes for the two-dimensional Riemann problems for the wave equation systems. Discrete Contin. Dyn. Syst. (A) *9* (2003), 559–576. Zbl 1032.65112

[7] *M. Lukáčová-Medviďová, K. W. Morton, and G. Warnecke*: Evolution Galerkin methods for hyperbolic systems in two space dimensions. Math. Comput. *69* (2000), 1355–1384. Zbl 0951.35076

[8] *M. Lukáčová-Medviďová, K. W. Morton, and G. Warnecke*: Finite volume evolution Galerkin methods for Euler equations of gas dynamics. Internat. J. Numer. Methods Fluids *40* (2002), 425–434. Zbl 1023.76026

[9] *M. Lukáčová-Medviďová, K. W. Morton, and G. Warnecke*: Finite volume evolution Galerkin (FVEG) methods for hyperbolic systems. SIAM J. Sci. Comput. *26* (2004), 1–30. Zbl pre 02138731

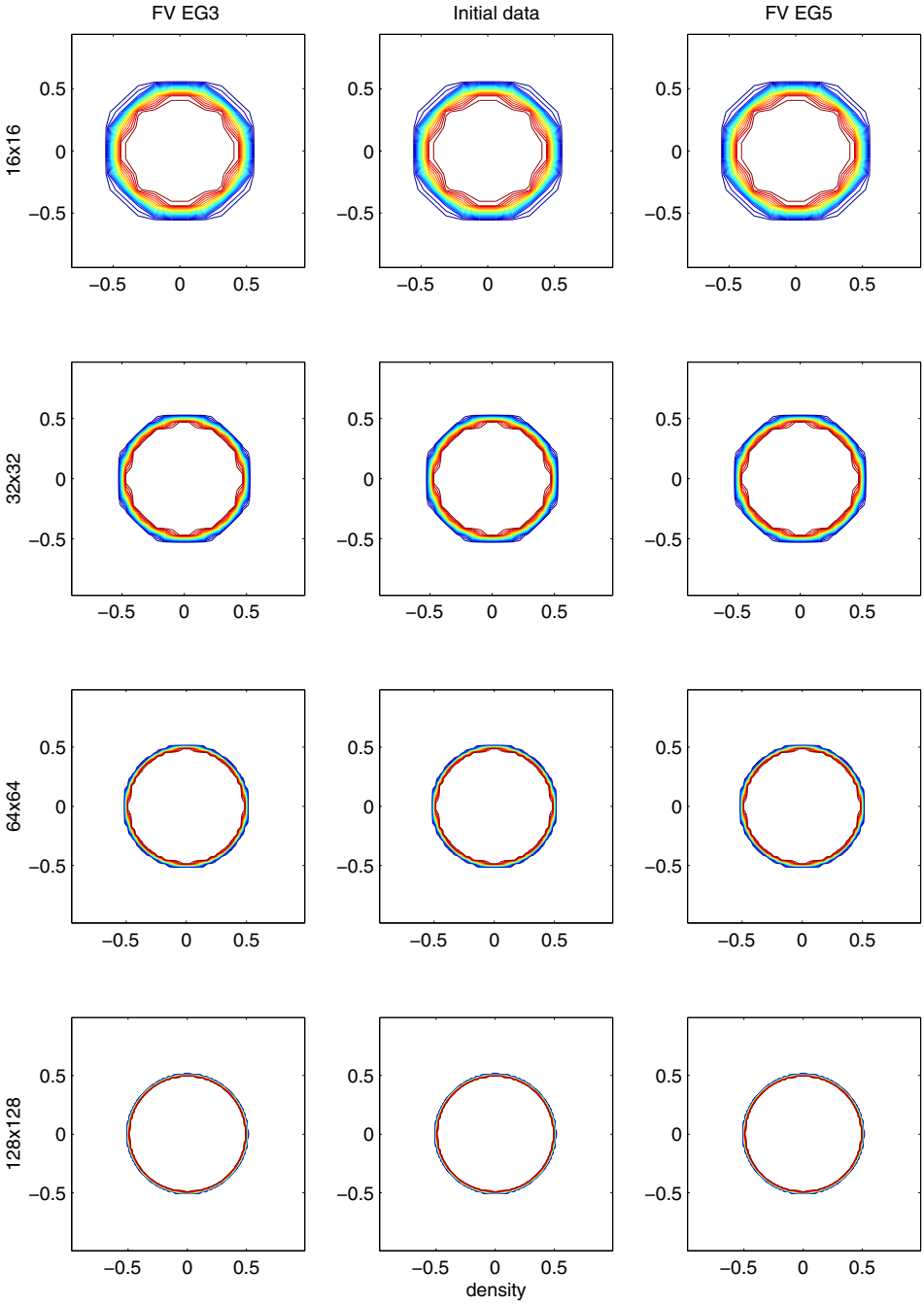

Figure 4. Static disc problem; plots of density isolines on different meshes.

[10] *M. Lukáčová-Medviďová, J. Saibertová, and G. Warnecke*: Finite volume evolution Galerkin methods for nonlinear hyperbolic systems. J. Comput. Phys. *183* (2002), 533–562. Zbl pre 01901722

[11] *M. Lukáčová-Medviďová, G. Warnecke*: Lax-Wendroff type second order evolution Galerkin methods for multidimensional hyperbolic systems. East-West Numer. Math. *8* (2000), 127–152. Zbl 0959.65104

[12] *M. Lukáčová-Medviďová, G. Warnecke, and Y. Zahaykah*: On the stability of the evolution Galerkin schemes applied to a two-dimensional wave equation system. SIAM J. Numer. Anal. (2006). In print. Zbl

[13] *K. W. Morton*: On the analysis of finite volume methods for evolutionary problems. SIAM J. Numer. Anal. *35* (1998), 2195–2222. Zbl 0927.65119

[14] *S. Noelle*: The MOT-ICE: a new high-resolution wave-propagation algorithm for multi-dimensional systems of conservative laws based on Fey's method of transport. J. Comput. Phys. *164* (2000), 283–334. Zbl 0967.65100

[15] *S. Ostkamp*: Multidimensional characterisitic Galerkin schemes and evolution operators for hyperbolic systems. Math. Methods Appl. Sci. *20* (1997), 1111–1125. Zbl

[16] *S. Ostkamp*: Multidimensional characteristic Galerkin schemes and evolution operators for hyperbolic systems. PhD. thesis. University Hannover, 1995. Zbl

[17] *J. Saibertová*: Genuinely multidimensional finite volume schemes for systems of conservation laws. PhD. thesis. Technical University Brno, 2003. Zbl

[18] *Y. Zahaykah*: Evolution Galerkin schemes and discrete boundary conditions for multidimensional first order systems. PhD. thesis. University of Magdeburg, 2002. Zbl 1008.65073

Authors' addresses: *M. Lukáčová-Medviďová*, Institute of Numerical Simulation, Hamburg University of Technology, Schwarzenbergstraße 95, Hamburg, Germany, e-mail: `lukacova@tu-harburg.de`; *J. Saibertová-Zatočilová*, Institute of Mathematics, University of Technology Brno, Technická 2, CZ-616 00 Brno, Czech Republic, e-mail: `saibertova @um.fme.vutbr.cz`.